energy&fuels

Article

pubs.acs.org/EF

Nanofluid Enhanced Oil Recovery Using Hydrophobically Associative Zwitterionic Polymer-Coated Silica Nanoparticles

Sang Koo Choi,[†,‡] Han Am Son,[†,‡] Hyun Tae Kim,[§] and Jin Woong Kim*[,‡,∥]

[‡]Department of Bionano Technology and [∥]Department of Chemical and Molecular Engineering, Hanyang University, Ansan, Gyeonggi-do 15588, Republic of Korea

[§]Division of Petroleum and Marine Research, Korea Institute of Geoscience and Mineral Resources, Daejeon 34132, Republic of Korea

ABSTRACT: Intense interest has been shown in the development of "smart nanofluids" because they can dramatically change their flow properties in complex fluid systems. We introduce a robust and straightforward approach to develop a smart nanofluid system, in which associative silica nanoparticles (ASNPs) were incorporated to regulate their flow properties in rock pores. ASNPs were synthesized by covalently coating a hydrophobically associative hygroscopic zwitterionic poly[2-methacryloyloxyethyl phosphorylcholine (MPC)-*co*-divinylbenzene (DVB)] shell layer on 20 nm sized silica nanoparticles (NPs) by surface-mediated living radical polymerization. The essence of our approach is to copolymerize DVB, which endows the polymer shell of ASNPs with a weak long-range hydrophobic attraction. This leads to the favorable formation of a wedge film as a result of structural disjoining pressure. This wedge film made the oil adsorbed on the rock surface more dewettable, thus enhancing the efficiency of oil recovery. As a result of this unique behavior, the ASNP nanofluid developed in this study remarkably improved the fluidity of complex oil fluids; ∼5 vol % oil recovery enhancement and ∼0.3 psi pressure reduction were also achieved in comparison to neat nanofluid controls.

1. INTRODUCTION

High-performance fluid systems, including surfactant flooding,[1−4] polymer flooding,[5−7] particle-stabilized Pickering emulsions,[8−10] and nanofluids,[11−13] have been of great interest in enhanced oil recovery (EOR). One of the key technologies currently used for high oil recovery involves manipulating the wettability alteration between the oil and the rock surface, which is useful for the spontaneous influx of water into the rock, thus displacing the oil from the rock pore. In terms of creating a new type of fluid functionality, exploitation of smart nanofluids is intriguing for the oil industry because they dramatically regulate the fluidity with the sole aid of nano-objects. For this purpose, smart nanofluids have been fabricated by incorporating surface-functionalized nanospecies, such as inorganic nanoparticles (NPs),[14,15] carbon nanomaterials,[16,17] and nanofibers.[18,19] Dependent upon the surface chemistry, particle size, anisotropy, and particle−particle or particle−substrate interactions, they give rise to totally different mechanical, thermal, electrical, magnetic, and rheological fluid behaviors, which would make the oil fluid more recoverable from the reservoir. Their shear stress-dependent rheological property facilitates oil recovery, while the oil mixture travels through the rock pore channel.

Recent advances in the EOR industry have opened new avenues for the fabrication of high-performance smart nanofluids. For example, smart nanofluids incorporated with alumina or zirconia NPs can alter the wetting conditions of reservoir rock cores from an oil-wet to a water-wet preference, thus increasing the recovery efficiencies of oil fluids. In addition, surface-modified NPs of smart nanofluids irreversibly attach to the oil−water interface in the rock pores and decrease the interfacial tension, thereby dramatically improving the oil recovery efficiency.[20,21] Despite these advances in engineering smart nanofluids, practical applications in the EOR industry are still hampered because the average diameter of rock pores (typically less than 100 nm) is too small to allow functional NPs to freely pass through them and play their own roles. Considering a clogging process of a pore channel with particles whose dimension is smaller than the pore channel, the degree of clogging increases in proportion to a decline in $(W/D)^m$, where W is the width of the pore, D is the diameter of the particle, and m is an experimental value of ≈4. A demonstration experiment has shown that, if the particles occupy more than 10% of the pore size, the pore channel would be readily clogged by them.[22] Further, when the NPs in the nanofluid are strongly attracted to each other, they can hardly display the designated surface functionality at the oil−rock surface interface, usually resulting in either complete segregation from the fluid or blocking of the pore channel.[23,24] To avoid such problems, the NPs should have a much smaller particle size than the rock pores while activating the rock surface with a controlled degree of interaction.

The ultimate goal of this study is to synthesize hydrophobically attractive silica nanoparticles (ASNPs) that can be incorporated in a smart nanofluid system for EOR. ASNPs were synthesized by covalently coating a hydrophobically modified poly(2-methacryloyloxyethyl phosphorylcholine-*co*-divinylbenzne), hereafter referred to as poly(MPC-*co*-DVB), on 20 nm sized silica NPs by surface-mediated living radical polymerization. The degree of hydrophobic attraction was

Received: February 15, 2017
Revised: May 18, 2017
Published: May 24, 2017

DOI: 10.1021/acs.energyfuels.7b00455
Energy Fuels 2017, 31, 7777−7782

controlled by changing the copolymerization ratio of DVB/MPC. MPC was used as a zwitterionic monomer to impart a strong hygroscopic nature to the polymer shell.[25,26] Basically, ASNPs synthesized in this study could hydrophobically associate with each other as a result of the weak but effective attractive nature of the polymer shell. Finally, we tried to demonstrate that our ASNPs were useful in providing a controlled attractive force to the nanofluid system, which eventually led to EOR.

2. EXPERIMENTAL SECTION

2.1. Materials. 2-Methacryloyloxyethyl phosphorylcholine (MPC) was supplied by KCI Co. (Korea). Ethanol (99.9%) and *n*-decane (99.0%) were supplied by Daejung (Korea). Tetrahydrofuran (THF, >98%) and trichloroacetyl isocyanate (>98%) were purchased from TCI (Japan). Ludox CL-X colloidal silica (45 wt % suspension in water), fluorescein isothiocyanate (FITC, >90%), (3-aminopropyl)-triethoxysilane (APS, >98%), dibutyltin dilaurate (95%), molybdenum hexacarbonyl [$Mo(CO)_6$, 98%], and divinylbenzene (55%) were purchased from Sigma-Aldrich (St. Louis, MO, U.S.A.). All of the other chemicals were of reagent grade and used without further purification.

2.2. Grafting Poly(MPC-*co*-DVB) on Silica NPs. Using surface-mediated living radical polymerization, hydrophobically associative poly(MPC-*co*-DVB) was chemically coated on silica NPs. To provide initiation sites, amino groups were attached on the surface of silica NPs by the reaction of APS with silanol groups.

In a typical synthetic procedure, silica NPs (0.5 g) and 150 mL of toluene containing 5 wt % APS were charged in a 250 mL round-bottom flask equipped with a reflux condenser, a mechanical stirrer, and an argon inlet system. The reaction mixture was refluxed at 110 °C for 8 h while gently stirring with a mechanical stirrer. After treatment, the resulting mixture was repeatedly centrifuged at 4000 rpm for 5 min with THF and dried under vacuum at ambient temperature. The urea condensation reaction between trichloroacetyl isocyanate and amino groups on the surface of the silica NPs was carried out in a round-bottom flask. APS-treated silica NPs (4.0 g), trichloroacetyl isocyanate (1.0 g), and 150 mL of toluene were charged in the flask, and the mixture was stirred at 80 °C for 8 h under argon. After the reaction, the product, silica−$COCCl_3$, was recovered by centrifugation at 4000 rpm for 5 min with THF. Finally, to graft poly(MPC-*co*-DVB) onto the silica NPs, silica−$COCCl_3$ (1.0 g), $Mo(CO)_6$ (0.02 g), MPC/DVB (1.0 g, with the copolymerization ratio being relatively varied against the total monomer mass), and 100 mL of ethanol were charged. Polymerization was conducted at 70 °C for 12 h under an argon atmosphere. After polymerization, the product was repeatedly centrifuged at 4000 rpm for 5 min with methanol. Finally, the ASNPs were transferred to water.

2.3. Morphological and Interfacial Characterization of ASNPs. Transmission electron microscopy (TEM, JEM-2100F, JEOL, Japan) was used to observe the shape and size of the ASNPs. The measurement was performed with an acceleration voltage of 200 kV and a probe size under 0.5 nm. The shell mass and thermal stability of ASNPs were assessed via thermogravimetric analysis (TGA, TGA Q500, TA Instruments, New Castle, DE, U.S.A.). For this, the ASNPs were dried for 48 h at 70 °C under vacuum. The sample was heated to 800 °C in air at a heating rate of 20 °C/min. To evaluate the adsorption behavior of ASNPs at the interface, we measured the interfacial tension at the interface of *n*-decane and water with a tensiometer (Sigma 700, KSV, Sweden). In these measurements, Ludox CL-X and ASNPs were finely dispersed in the water phase (0.05 wt %) by sonication.

2.4. Characterization of Nanofluids. The hydration ability of the ASNP was evaluated by measuring the weight loss of the aqueous nanofluid using a thermohygrostat (THRT-P300, Korea). The test was conducted at a precisely controlled temperature (40 °C) and humidity (30%). For suspension rheology studies, the ASNPs were finely dispersed in water with the aid of a probe-type sonicator (VCX130, Sonics & Materials, Inc., Newtown, CT, U.S.A.). Pulsatile sonication was applied at 130 W for 2 min with a time interval of 1 s. The rheological properties of the ASNP nanofluids were characterized with a DHR1 rheometer (TA Instruments, New Castle, DE, U.S.A.). This rheometer was equipped with a 40 mm cone−plate with a cone angle of 1°. The nanofluids only contained 45 wt % ASNPs in water. The nanofluid sample (1 mL) was then carefully dispensed onto the rheometer plate. The viscosity was measured while changing the shear rate from 0.1 to 100 s^{-1}. All measurements were carried out at room temperature.

2.5. Lab-Scale Oil Recovery Test. The experimental apparatus consisted of an injection pump (500D syringe pump, Teledyne Isco, Lincoln, NE, U.S.A.), an accumulator (CFR-100, TEMCO, Inc., Tulsa, OK, U.S.A.), a core holder (Toung-sung Tech, Korea), and a measuring cylinder. The nanofluid was injected into the core holder through the accumulator, and the influx flow lines from the accumulator were connected to the core holder packed with Berea sandstone. After the nanofluid flowed through the pores of the sandstone, the recovered fluid was collected in the measuring cylinder. In this process, the nanofluid was injected at 1 cm^3/min (corresponding to a Darcy velocity of 9.3 ft/day) using the injection pump. Pressure transducers (DXD, Heise, Stratford, CT, U.S.A.) were installed at the inlet and outlet of the core holder to monitor pressure transitions. All measurements were conducted at 25 °C.

3. RESULTS AND DISCUSSION

ASNPs were synthesized by surface-mediated living radical polymerization, as schematically shown in Figure 1A. ASNPs

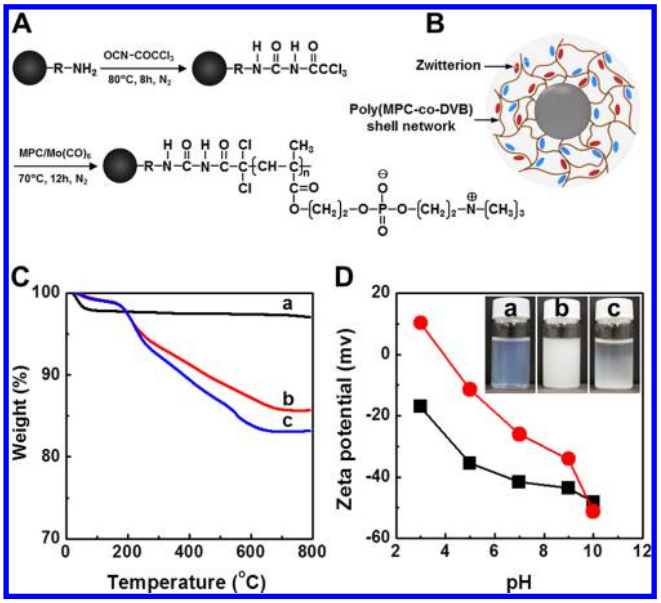

Figure 1. (A) Schematic presentation for synthesis of ASNPs. (B) Graphical representation of an ASNP. (C) TGA of (a) Ludox CL-X and ASNPs with (b) ϕ_{DVB} = 0.09 and (c) ϕ_{DVB} = 0.17. (D) ζ potential of ASNP nanofluids with varying pH: (black squares) Ludox CL-X and (red circles) ASNPs with ϕ_{DVB} = 0.17. The insets are the images of (a) Ludox CL-X, (b) ASNPs on preparation, and (c) ASNPs after 12 h of storage at room temperature.

are structured with a poly(MPC-*co*-DVB) shell (Figure 1B). From the TGA (Figure 1C), the monomer conversion to the poly(MPC-*co*-DVB) shell was measured to be 24−34%. Copolymerization of a higher weight fraction of DVB, ϕ_{DVB}, increased monomer conversion. This is because the more hydrophobic monomer leads to more favorable partitioning in the growing poly(MPC-*co*-DVB) gel network deposited on the silica NPs.[27] To figure out how the generation of the poly(MPC-*co*-DVB) shell affected the surface property of

DOI: 10.1021/acs.energyfuels.7b00455
Energy Fuels 2017, 31, 7777−7782

ASNPs, we investigated the ζ potential of ASNPs by varying the medium pH (Figure 1D). The ζ potential values of bare silica dispersion, Ludox CL-X, ranged from −17 to −48 mV over the pH from 3 to 10, which is a common result for negatively charged silica NPs. However, the ASNP nanofluid showed much higher ζ potentials than Ludox CL-X by the difference of nearly 30 mV. The ζ potential value of the ASNP nanofluid was even close to 0 as pH is lowered. These imply that the surface became hydrophobic by coating the surface with poly(MPC-*co*-DVB), which would stem from copolymerization of hydrophobic DVB. From the apparent dispersion stability, we were able to demonstrate that ASNPs gradually associate and eventually sediment after long-term storage, which is quite comparable to Ludox CL-X dispersion (inset of Figure 1D).

From high-resolution transmission electron microscopy (HR-TEM) analysis of the ASNPs, we directly characterized the thicknesses of the polymer shells. Ludox CL-X showed a clean surface topology with no phase adhesion between the particles (Figure 2A). In contrast, ASNPs fabricated using 20 nm Ludox CL-X were glued to each other with a squishy phase while maintaining their spherical shape. This reveals that a thin poly(MPC-*co*-DVB) shell was successfully generated at the periphery of silica NPs (Figure 2B). When ASNPs were synthesized using 100 nm sized silica NPs, the polymer shell could be more clearly observed with a shell thickness of tens of nanometers (Figure 2C). From the direct transmission electron microscopy (TEM) analysis, we measured the changes in particle diameter with an increasing monomer concentration (Figure 2D). The average diameter of ASNPs increased in a monomer concentration-dependent manner. Considering the diameters of bare silica NPs, the ASNPs produced using our fabrication recipe had polymer shells whose thickness ranged to a few nanometers in dry conditions. These results elucidate that surface-mediated living radical polymerization was successfully performed to generate a thin poly(MPC-*co*-DVB) shell layer.

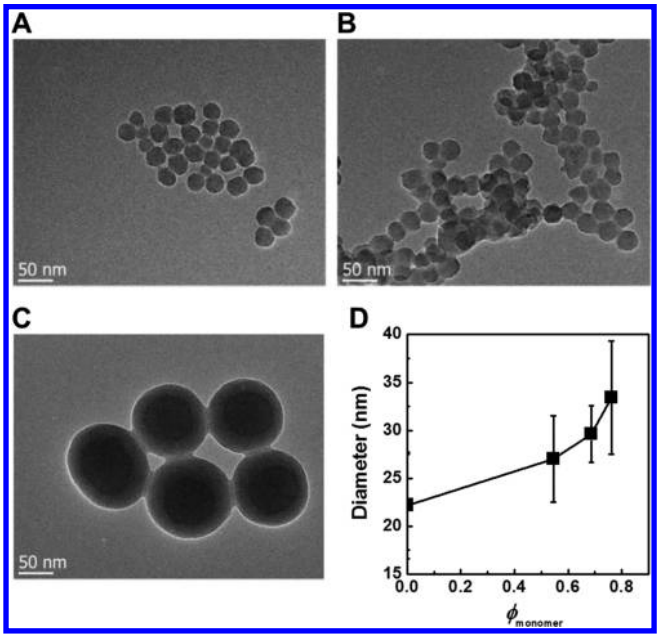

Figure 2. Transmission electron microscope images of (A) Ludox CL-X and ASNPs synthesized using (B) 20 nm sized silica NPs and (C) 100 nm sized silica NPs. (D) Particle size changes with the increase of the concentration of grafting monomers. ASNPs with ϕ_{DVB} = 0.17 were used for this observation.

Feasible tuning of ϕ_{DVB} would endow ASNPs with the ability to tune the degree of hydrophobic association in the aqueous phase. To confirm this, we directly characterized the interfacial activity of ASNPs by measuring the interfacial tension between *n*-decane and the aqueous phase containing them (Figure 3A).

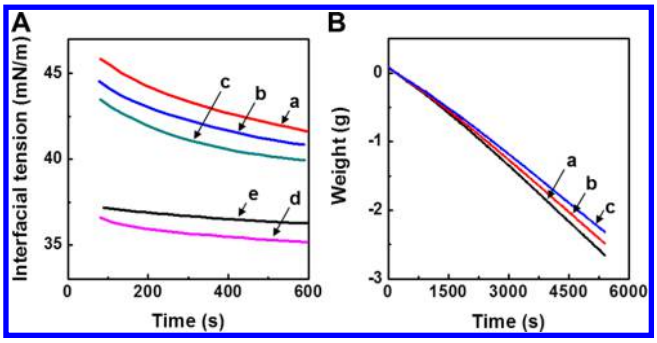

Figure 3. (A) Dynamic interfacial tension changes at the *n*-decane/water interface in the presence of ASNPs with (a) ϕ_{DVB} = 0.03, (b) ϕ_{DVB} = 0.05, (c) ϕ_{DVB} = 0.09, (d) ϕ_{DVB} = 0.17, and (e) pure *n*-decane/water interfacial tension. (B) Weight loss of aqueous nanofluids as a function of the storage time in a thermohygrostat: (a) water solution only and (b and c) ASNP nanofluid. ASNPs with (b) ϕ_{DVB} = 0.09 and (c) ϕ_{DVB} = 0.03 were used for this observation.

At low ϕ_{DVB}, the dynamic interfacial tension between *n*-decane and the aqueous solution was significantly higher than the case without ASNPs. As ϕ_{DVB} increased, the interfacial tension also gradually decreased. When ϕ_{DVB} was high enough, the interfacial tension was lower than that of the pure *n*-decane−water interface. This unprecedented interfacial tension behavior seemed to originate from the competition between hydration and hydrophobication of the poly(MPC-*co*-DVB) shell, depending upon its copolymerization stoichiometry. In other words, in the case of low ϕ_{DVB}, ASNPs can be completely hydrated because the hygroscopic MPC units readily took a lot of water molecules. As a result of this reason, the ASNPs would strengthen cohesion of water molecules at the oil−water interface, thus increasing the interfacial tension. On the other hand, when ϕ_{DVB} was high enough, the interfacial tension was rather lower than the case without ASNPs, which is because the divinylbenzene unit made the polymer shell phase hydrophobic.

To experimentally confirm this peculiar behavior, we observed the evaporation behavior of water molecules in the presence of ASNPs in a temperature- and humidity-controlled thermohygrostat (Figure 3B). The results showed that the presence of ASNPs in the aqueous phase dramatically retarded water evaporation compared to the controls. This indicates that the ASNPs acted like nanoscale salts that strongly hold water molecules, producing more cohesive energy to the aqueous phase, which consequently increases the interfacial tension. As ϕ_{DVB} increased, the DVB would make the polymer shell relatively hydrophobic, which enables the effective adhesion of ASNPs onto the oil−water interface. Judging from the suspension state of ASNPs in water, we can conclude that, even though the polymer shell is hydrophobically modified by copolymerizing DVB, the ASNPs were fully hydrated in the aqueous media. If not, all of the ASNPs would aggregate to form a separated phase, which was not observed in our study.

Inspired by the successful synthesis of ASNPs, we tried to characterize the hydrophobic attraction between the ASNPs in

DOI: 10.1021/acs.energyfuels.7b00455
Energy Fuels 2017, 31, 7777−7782

the aqueous phase. One of the most reliable methods for characterization of the particle−particle interaction is dense suspension rheology. Studies have shown that, in dense suspension conditions, the distance between particles is so short that the fluidity would be changed by the presence of any particle−particle interaction. To confirm this, we concentrated bare silica NPs and ASNPs to exactly 45 wt % in water and their viscosity versus shear rate and storage modulus versus strain curves were obtained. The viscosity over the shear rate variation of the dense ASNP nanofluid was approximately 2 orders of magnitude higher than that of the bare silica nanofluid (Figure 4A). The storage modulus also showed a similar pattern over

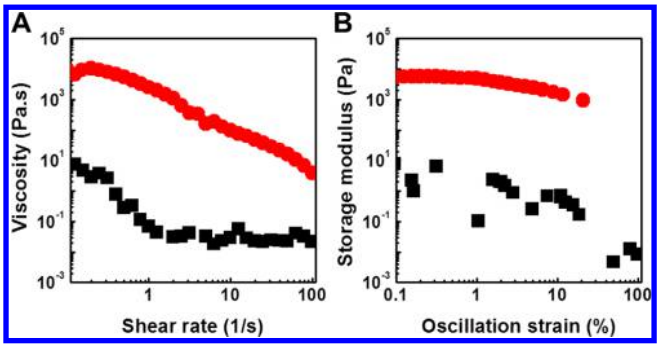

Figure 4. (A) Viscosity versus shear rate curves and (B) storage modulus versus oscillation strain for ASNP nanofluids: (black squares) Ludox CL-X and (red circles) ASNPs with ϕ_{DVB} = 0.17. The concentration of NPs was exactly tuned to be 45 wt % in the aqueous dispersion.

the strain variation (Figure 4B). These different rheological behaviors of the ASNP nanofluid must stem from the formation of a three-dimensional colloidal gel network in water as a result of the hydrophobic interaction between the poly(MPC-*co*-DVB) shells. It was also obvious in our rheology studies that the viscosity curve of the ASNP nanofluid showed typical shear thinning behavior. This arises from the breakdown of the colloidal gel network structure in response to the applied shear stress. However, upon removal of the shear stress, the gel network structure was recovered. This rheological behavior would likely enable the ASNP nanofluid to flow through the rock core under confining pressure.

To investigate how injection of the ASNP nanofluid affects oil recovery from sandstone, we conducted the core flooding experiment with the injection of pure water, bare silica NP nanofluid, and ASNP nanofluid into Berea sandstone (Figure 5). In this experiment, we used the nanofluid containing the ASNPs with ϕ_{DVB} = 0.17, because its interfacial tension was lower than the tension at the pure *n*-decane−water interface, thus enhancing miscible displacement. Our core flooding experiment showed that, when the ASNP nanofluid was injected, 74.1% oil was recovered, which is quite comparable to cases using water only (68.9%) and unmodified NPs (72.7%) (Figure 6A). From the investigation of pressure variance between inlet and outlet in the sandstone during the core flooding, it was interesting to observe that the injection of the ASNP nanofluid significantly lowered the pressure relative to the injection of the bare silica NP nanofluid (Figure 6B). Considering that the particle size of ASNP is bigger than that of the bare silica NP, ASNPs would have a higher possibility to clog the pore channel, thereby increasing the pressure variance before and after injection. However, the reverse was the result.

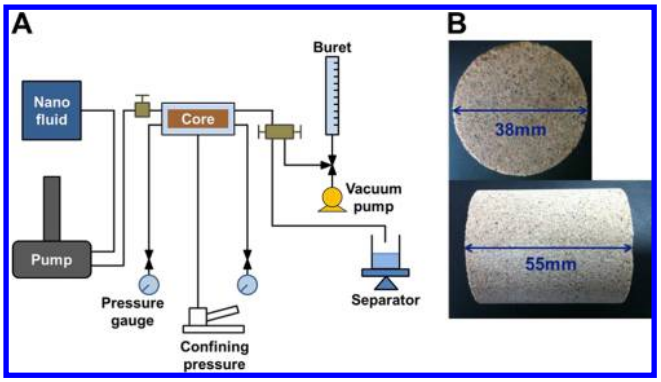

Figure 5. (A) Schematic presentation for the characterization of oil recovery. (B) Photographs of Berea sandstone used in the experiment: (top) top view and (bottom) side view.

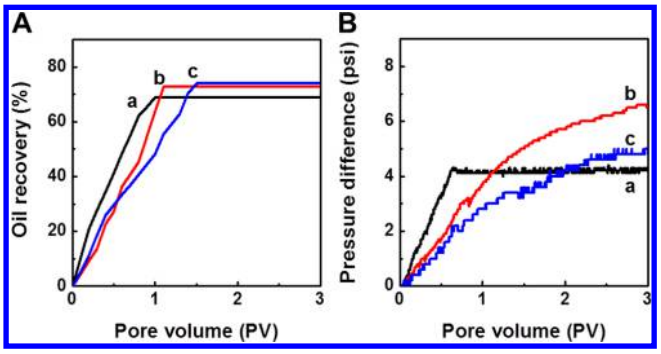

Figure 6. (A) Oil recovery as a function of the pore volume (PV). PV is the relative volume of an injection fluid that is normalized by the total pore volume of the rock sample. (B) Pressure variation as a function of PV: (a) water injection throughout 3 PV, (b) Ludox CL-X injection throughout 3 PV, and (c) ASNP nanofluid injection throughout 3 PV. ASNPs with ϕ_{DVB} = 0.17 were used.

This implies that ASNPs play a role in improving fluidity while traveling through the pores of Berea sandstone.

Considering these results, we assumed that ASNPs altered the inner surface conditions of sandstone into more hydrophilic conditions during the injection of the nanofluid. To elucidate the behavior of ASNPs at the oil−rock interface, a model experiment was developed, in which we placed drops of *n*-decane in a glass capillary tube filled with the ASNP nanofluid and microscopically monitored how the ASNPs behave at the wedge regime when *n*-decane drops on the glass surface. We observed a favorable formation of a colloidal film at the wedge regime, which is usually referred to as the wedge film (Figure 7).[28−30] As demonstrated, the poly(MPC-*co*-DVB) shell of ASNPs is hydrophobically attractive, allowing ASNPs to weakly interact with each other while displaying electrostatic repulsion against the rock surface wetted by the aqueous phase. Such weak but long-range hydrophobic attraction of ASNPs would lead to favorable formation of the wedge film, caused by structural disjoining pressure, thus causing influx of the nanofluid into the oil-wet glass surface. This wedge film readily altered the wettability of the oil drop against the glass surface. This model experiment highlights that the oil phase adsorbed on the rock surface could be effectively extracted by the injection of ASNP nanofluid, thus enhancing oil recovery.

DOI: 10.1021/acs.energyfuels.7b00455
Energy Fuels 2017, 31, 7777−7782

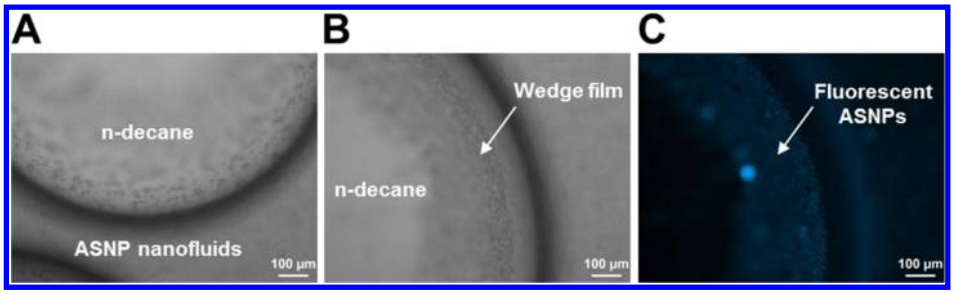

Figure 7. Microscopic observations for the formation of a colloidal wedge film formation at the interface of *n*-decane and nanofluids. Bright-field microscope images (A) on preparation and (B) after 60 s. (C) Fluorescence microscope image for the wedge film. For this observation, ASNPs were tagged with FITC. ASNPs with ϕ_{DVB} = 0.17 were used for this experiment.

4. CONCLUSION

In this study, we introduced a technology to develop a smart nanofluid system for enhancing oil recovery. The key of our approach was to synthesize hydrophobically attractive zwitterionic poly(MPC-*co*-DVB) shell-coated silica nanoparticles, ASNPs. The degree of hydrophobic attractiveness of the shell polymer was controlled by regulating the copolymerization ratio of DVB against hygroscopic MPC. We experimentally confirmed that the ASNPs could change the interfacial tension at the oil−water interface and display water retention performance, which is attributed to the surface chemistry of the polymer shell. Moreover, the dense suspension rheology study confirmed that the ASNPs had particle−particle attraction. The core flooding experiment demonstrated that the ASNP nanofluid could enhance oil recovery by ∼5 vol % while lowering the injection pressure, which is closely related to the formation of the wedge film between the oil and the rock surface. These results highlight that the ASNP nanofluid developed in this study is a potential injection agent that can enhance oil recovery by altering the wettability of the oil drop against the rock pore surface.

AUTHOR INFORMATION

Corresponding Author

*Fax: +82-31-400-5457. E-mail: kjwoong@hanyang.ac.kr.

ORCID

Jin Woong Kim: 0000-0002-2823-8825

Author Contributions

†Sang Koo Choi and Han Am Son contributed equally to this work.

Notes

The authors declare no competing financial interest.

ACKNOWLEDGMENTS

This research was supported by National Research Foundation of Korea (NRF) grants funded by the Ministry of Science, Information and Communications Technology (ICT) and Future Planning (MSIP) of the Korean government (2008-0061891 and 2016R1A2B2016148).

REFERENCES

(1) Zargartalebi, M.; Kharrat, R.; Barati, N. Enhancement of surfactant flooding performance by the use of silica nanoparticles. *Fuel* **2015**, *143*, 21−27.

(2) ShamsiJazeyi, H.; Verduzco, R.; Hirasaki, G. J. Reducing adsorption of anionic surfactant for enhanced oil recovery: Part I. Competitive adsorption mechanism. *Colloids Surf., A* **2014**, *453*, 162−167.

(3) Ko, K. M.; Chon, B. H.; Jang, S. B.; Jang, H. Y. Surfactant flooding characteristics of dodecyl alkyl sulfate for enhanced oil recovery. *J. Ind. Eng. Chem.* **2014**, *20* (1), 228−233.

(4) Park, S.; Lee, E. S.; Sulaiman, W. R. W. Adsorption behaviors of surfactants for chemical flooding in enhanced oil recovery. *J. Ind. Eng. Chem.* **2015**, *21*, 1239−1245.

(5) Pei, H.; Zhang, G.; Ge, J.; Zhang, L.; Wang, H. Effect of polymer on the interaction of alkali with heavy oil and its use in improving oil recovery. *Colloids Surf., A* **2014**, *446*, 57−64.

(6) Zhao, P.; Gao, B.; Xu, S.; Kong, J.; Ma, D.; Shon, H. K.; Yue, Q.; Liu, P. Polyelectrolyte-promoted forward osmosis process for dye wastewater treatment—Exploring the feasibility of using polyacrylamide as draw solute. *Chem. Eng. J.* **2015**, *264*, 32−38.

(7) Veerabhadrappa, S. K.; Trivedi, J. J.; Kuru, E. Visual Confirmation of the elasticity dependence of unstable secondary polymer floods. *Ind. Eng. Chem. Res.* **2013**, *52* (18), 6234−6241.

(8) Lee, G. J.; Son, H. A.; Cho, J. W.; Choi, S. K.; Kim, H. T.; Kim, J. W. Stabilization of Pickering emulsions by generating complex colloidal layers at liquid−liquid interfaces. *J. Colloid Interface Sci.* **2014**, *413*, 100−105.

(9) Cui, Z. G.; Cui, C. F.; Zhu, Y.; Binks, B. P. Multiple phase inversion of emulsions stabilized by in situ surface activation of $CaCO_3$ nanoparticles via adsorption of fatty acids. *Langmuir* **2012**, *28* (1), 314−320.

(10) Son, H. A.; Yoon, K. Y.; Lee, G. J.; Cho, J. W.; Choi, S. K.; Kim, J. W.; Im, K. C.; Kim, H. T.; Lee, K. S.; Sung, W. M. The potential applications in oil recovery with silica nanoparticle and polyvinyl alcohol stabilized emulsion. *J. Pet. Sci. Eng.* **2015**, *126*, 152−161.

(11) Al-Anssari, S.; Barifcani, A.; Wang, S.; Maxim, L.; Iglauer, S. Wettability alteration of oil-wet carbonate by silica nanofluid. *J. Colloid Interface Sci.* **2016**, *461*, 435−442.

(12) Hashemi, R.; Nassar, N. N.; Pereira Almao, P. Nanoparticle technology for heavy oil in-situ upgrading and recovery enhancement: Opportunities and challenges. *Appl. Energy* **2014**, *133*, 374−387.

(13) Wang, F.-C.; Wu, H.-A. Enhanced oil droplet detachment from solid surfaces in charged nanoparticle suspensions. *Soft Matter* **2013**, *9* (33), 7974−7980.

(14) Shen, B.; Ma, Y.; Yu, S.; Ji, C. Smart multifunctional magnetic nanoparticle-based drug delivery system for cancer thermo-chemotherapy and intracellular imaging. *ACS Appl. Mater. Interfaces* **2016**, *8* (37), 24502−24508.

(15) Liong, M.; Lu, J.; Kovochich, M.; Xia, T.; Ruehm, S. G.; Nel, A. E.; Tamanoi, F.; Zink, J. I. Multifunctional inorganic nanoparticles for imaging, targeting, and drug delivery. *ACS Nano* **2008**, *2* (5), 889−896.

(16) Kalinina, I.; Worsley, K.; Lugo, C.; Mandal, S.; Bekyarova, E.; Haddon, R. C. Synthesis, dispersion, and viscosity of poly(ethylene glycol)-functionalized water-soluble single-walled carbon nanotubes. *Chem. Mater.* **2011**, *23* (5), 1246−1253.

(17) Lei, Y.; Xiong, C.; Guo, H.; Yao, J.; Dong, L.; Su, X. Controlled viscoelastic carbon nanotube fluids. *J. Am. Chem. Soc.* **2008**, *130* (11), 3256−3257.

(18) Liang, H. W.; Guan, Q. F.; Chen, L. F.; Zhu, Z.; Zhang, W. J.; Yu, S. H. Macroscopic-scale template synthesis of robust carbonaceous

DOI: 10.1021/acs.energyfuels.7b00455
Energy Fuels 2017, 31, 7777−7782

nanofiber hydrogels and aerogels and their applications. *Angew. Chem., Int. Ed.* **2012**, *51* (21), 5101−5105.
(19) Zhang, T.; Wang, W.; Zhang, D.; Zhang, X.; Ma, Y.; Zhou, Y.; Qi, L. Biotemplated synthesis of gold nanoparticle−bacteria cellulose nanofiber nanocomposites and their application in biosensing. *Adv. Funct. Mater.* **2010**, *20* (7), 1152−1160.
(20) Ferdous, S.; Ioannidis, M. A.; Henneke, D. E. Effects of temperature, pH, and ionic strength on the adsorption of nanoparticles at liquid−liquid interfaces. *J. Nanopart. Res.* **2012**, *14* (850), 1−12.
(21) Fan, H.; Striolo, A. Nanoparticle effects on the water−oil interfacial tension. *Phys. Rev. E: Stat. Nonlin. Soft Matter Phys.* **2012**, *86* (5), 051610.
(22) Wyss, H. M.; Blair, D. L.; Morris, J. F.; Stone, H. A.; Weitz, D. A. Mechanism for clogging of microchannels. *Phys. Rev. E: Stat. Nonlin. Soft Matter Phys.* **2006**, *74* (6), 061402.
(23) Bacchin, P.; Derekx, Q.; Veyret, D.; Glucina, K.; Moulin, P. Clogging of microporous channels networks: Role of connectivity and tortuosity. *Microfluid. Nanofluid.* **2014**, *17* (1), 85−96.
(24) Habibi, A.; Ahmadi, M.; Pourafshary, P.; Ayatollahi, S.; Al-Wahaibi, Y. Reduction of fines migration by nanofluids injection: An experimental study. *SPE J.* **2013**, *18* (02), 309−318.
(25) Sangsuwan, A.; Kawasaki, H.; Matsumura, Y.; Iwasaki, Y. Antimicrobial silver nanoclusters bearing biocompatible phosphorylcholine-based zwitterionic protection. *Bioconjugate Chem.* **2016**, *27* (10), 2527−2533.
(26) Iwasaki, Y.; Ishihara, K. Cell membrane-inspired phospholipid polymers for developing medical devices with excellent biointerfaces. *Sci. Technol. Adv. Mater.* **2012**, *13* (6), 064101.
(27) Ueda, T.; Oshida, H.; Kurita, K.; Ishihara, K.; Nakabayashi, N. Preparation of 2-methacryloyloxyethyl phosphorylcholine copolymers with alkyl methacrylates and their blood compatibility. *Polym. J.* **1992**, *24*, 1259−1259.
(28) Nikolov, A.; Kondiparty, K.; Wasan, D. Nanoparticle self-structuring in a nanofluid film spreading on a solid surface. *Langmuir* **2010**, *26* (11), 7665−7670.
(29) Liu, K. L.; Kondiparty, K.; Nikolov, A. D.; Wasan, D. Dynamic spreading of nanofluids on solids part II: Modeling. *Langmuir* **2012**, *28* (47), 16274−16284.
(30) Wasan, D. T.; Nikolov, A. D. Spreading of nanofluids on solids. *Nature* **2003**, *423* (6936), 156−159.

DOI: 10.1021/acs.energyfuels.7b00455
Energy Fuels 2017, 31, 7777−7782